Journal of Solid State Chemistry **167,** 330–336 (2002)
doi:10.1006/jssc.2002.9537

Inorganic–Organic Hybrid Materials: Hydrothermal Synthesis and Characterization of the Metal Diphosphonates $M_2(O_3PCH_2C_6H_4CH_2PO_3)\cdot 2H_2O$ (M = Mn, Ni, Cd)

N. Stock[1] and T. Bein

Department Chemie, Ludwig-Maximilians-Universität München, Butenandtstr. 5-13 (Haus E), 81377 München, Germany

Received October 18, 2001; in revised form January 30, 2002; accepted February 8, 2002; published online March 27, 2002

IN HONOR OF PROFESSOR GALEN STUCKY ON THE OCCASION OF HIS 65TH BIRTHDAY

The three isostructural transition metal diphosphonates $M_2(O_3PCH_2C_6H_4CH_2PO_3)\cdot 2H_2O$ (M = Mn, Ni, Cd) were hydrothermally synthesized using *p*-xylenediphosphonic acid and the corresponding metal salts. The structures were refined in the orthorhombic space group $Pca2_1$ from X-ray powder diffraction data: $Mn_2(O_3PCH_2C_6H_4CH_2PO_3)\cdot 2H_2O$ (1): $a = 983.71(7)$, $b = 582.72(4)$, $c = 2173.5(2)$ pm, $V = 1245.8(1)\ 10^6$ pm, $Z = 4$, $wR_p = 0.079$, $R_p = 0.062$, $R_F = 0.081$; $Ni_2(O_3PCH_2C_6H_4CH_2PO_3)\cdot 2H_2O$ (2): $a = 951.18(3)$, $b = 562.31(2)$, $c = 2178.47(6)$ pm, $V = 1165.2(1)\ 10^6$ pm, $Z = 4$, $wR_p = 0.072$, $R_p = 0.054$, $R_F = 0.095$; $Cd_2(O_3PCH_2C_6H_4CH_2PO_3)\cdot 2H_2O$ (3): $a = 1005.19(3)$, $b = 594.37(2)$, $c = 2186.08(8)$, $V = 1304.3(1)\ 10^6$ pm, $Z = 4$, $wR_p = 0.067$, $R_p = 0.052$, $R_F = 0.059$. The structures are built up from corner-linked [MO_6] polyhedra (M = Mn, Ni, Cd) forming inorganic metal oxide layers. These layers are linked by the organic diphosphonic acids acting as pillars. Magnetization measurements of 1 confirm the presence of divalent ions and indicate antiferromagnetic ordering at low temperatures. Thermogravimetric as well as IR spectroscopic studies are also presented. © 2002 Elsevier Science (USA)

Key Words: **manganese; nickel; cadmium; phosphonate; hybrid material; hydrothermal synthesis; magnetic properties; IR spectroscopy; X-ray diffraction; Rietveld refinement.**

INTRODUCTION

Open-framework hybrid materials with organic and inorganic moieties are an attractive field of research due to their composite properties and the possibility of tuning their chemistry (1). The potential of these hybrid materials lies in their use as sorbents, ion exchangers, catalysts or charge storage materials. The use of bifunctional anionic units in this field (2) e.g., diphosphonates ($[O_3P–R–PO_3]^{4-}$) (3), aminophosphonates ($[O_3P–R–NH_2]^{2-}$) (4), and phosphonocarboxylates ($[O_3P–R–COO]^{3-}$) (5) has led to many new three-dimensional compounds. Most often pillared materials are observed and the layer distance can be tuned by the length and size of the alkyl or aryl group.

Mono and diphosphonates of metal(II) ions have been described in the literature (6) and especially with zinc and copper, many new materials have been obtained (7). Other divalent ions such as Fe (8), Co (3a), Mn (3d), and Ba (9) have also been used and have led to new compounds with interesting structures. Recent developments in this field include the synthesis of mixed metal phosphonates, which are supposed to exhibit interesting magnetic properties (10) and the use of triphosphonic acids (11) to expand further the phosphonate chemistry. In contrast, only little is known about nickel and cadmium diphosphonates. To our knowledge, there is only one study of nickel diphosphonate materials $Ni_4(O_3PCH_2PO_3)_2\cdot nH_2O$ ($n = 3, 2, 0$) (12) and there are no reports of a crystal structure determination of a cadmium diphosphonate. *Para*-xylenediphosphonic acid has been shown to be useful in the synthesis of copper diphosphonate $Cu_2(O_3PCH_2C_6H_4CH_2PO_3)\cdot 2H_2O$ (7a), but no other metal(II) compounds have been described yet. Recently, we have obtained structural data on $H_2O_3PCH_2C_6H_4CH_2PO_3H_2$ and $Co_2(O_3PCH_2C_6H_4CH_2PO_3)\cdot 2H_2O$ (14). In this paper we present hydrothermal synthesis and structural elucidation, as well as the thermal and magnetic properties, of the three diphosphonates, $M_2(O_3PCH_2C_6H_4CH_2PO_3)\cdot 2H_2O$ (M = Mn, Ni, Cd).

EXPERIMENTAL

Synthesis

The *p*-xylenediphosphonic acid was synthesized by a classical Arbuzov reaction followed by acidic hydrolysis of the ester of diphosphonic acid (13).

The three title compounds $Mn_2(O_3PCH_2C_6H_4CH_2PO_3)\cdot 2H_2O$ (**1**), $Ni_2(O_3PCH_2C_6H_4CH_2PO_3)\cdot 2H_2O$ (**2**), and $Cd_2(O_3PCH_2C_6H_4CH_2PO_3)\cdot 2H_2O$ (**3**) were synthesized at 160°C as single-phase products by hydrothermal

[1] To whom the correspondence should be addressed. Fax: + 49-89-2180-7622. E-mail: norbert.stock@cup.uni-muenchen.de.

0022-4596/02 $35.00

reactions of *p*-xylenediphosphonic acid, $H_2O_3PCH_2C_6H_4CH_2PO_3H_2$, with $MnCl_2{\cdot}4H_2O$, $NiCl_2 \cdot 6H_2O$, or $CdCl_2 \cdot H_2O$, respectively. In a typical experiment, 59.4 mg (0.25 mmol) of $NiCl_2{\cdot}6H_2O$ and 66.5 mg (0.25 mmol) of *p*-xylenediphosphonic acid were mixed in 7 g water. The reaction mixture was stirred to homogeneity, transferred to a 23 mL PTFE bottle and sealed in a stainless-steel autoclave (Parr, USA). The reaction was carried out at 160°C for 48 h under autogenous pressure. The resulting single-phase product was filtered and washed thoroughly with deionized water. Compound **1** was similarly prepared from 49.5 mg (0.25 mmol) $MnCl_2{\cdot}4H_2O$ and 66.5 mg (0.25 mmol) *p*-xylenediphosphonic acid in 7 g water and compound **3** from 57.1 mg (0.25 mmol) $CdCl_2{\cdot}2.5H_2O$ and 66.5 mg (0.25 mmol) *p*-xylenediphosphonic acid in 5 g water.

Physical Characterization

IR spectra were recorded on a Bruker IFS 66v/S FTIR spectrometer in the spectral range 4000-400 cm^{-1} using the KBr disk method. Thermogravimetric analysis was performed on a simultaneous thermal analyzer Netzsch STA 409 under air (40 cm^3 min^{-1}, heating rate: 10°C min^{-1}) performing TG and DTA/DSC measurements. The three samples show very similar behaviour. They are stable up to 210°C without any weight loss. Above these temperatures one-step losses of 8.4, 8.5 and 6.8% are observed, which correspond to the departure of the water molecules (calcd. 8.8, 8.7, 7.3% for **1**, **2**, and **3**, respectively). Above 500°C, the pyrolysis of the organic part of the structures takes place. The magnetic susceptibility data for **1** were recorded over the temperature range 5–300 K using a SQUID magnetometer, Quantum Design Model 1802. The microcrystalline sample was zero-field cooled (z.f.c.) to 4 K and the magnetization was measured on heating to 300 K in an applied field of 5000 G.

TABLE 1
Crystallographic Data for $M_2(O_3PCH_2C_6H_4CH_2PO_3)\cdot 2H_2O$ (M = Mn, Ni, Cd)

	$M_2(O_3PCH_2C_6H_4CH_2PO_3)\cdot 2H_2O$		
	M = Mn	M = Ni	M = Cd
M_r (g mol^{-1})	408.0	415.55	492.98
Space group	$Pca2_1$ (no. 29)	$Pca2_1$ (no. 29)	$Pca2_1$ (no. 29)
Radiation, λ (pm)	70.930	154.06	70.930
Unit cell dimensions (22°C) (pm)	a = 983.71(7) b = 582.72(4) c = 2173.5(2)	a = 951.18(3) b = 562.31(2) c = 2178.47(6)	a = 1005.19(3) b = 594.37(2) c = 2186.08(8)
V(10^6 pm)	1245.8(1)	1165.2(1)	1304.3(1)
Z	4	4	4
ρ_{calc} (g cm^{-3})	2.175	2.369	2.507
Profile range	$2^\circ \le 2\theta \le 60^\circ$	$3^\circ \le 2\theta \le 80^\circ$	$2^\circ \le 2\theta \le 50^\circ$
No. of data points	5790	7500	4750
Obs. reflections	1864	344	1150
Atomic parameters	60	60	60
Displacem. factors	2	4	1
Profile parameters	16	16	16
R values	wR_p = 0.079 R_p = 0.062 R_F = 0.081	wR_p = 0.072 R_p = 0.054 R_F = 0.095	wR_p = 0.067 R_p = 0.052 R_F = 0.059

TABLE 2
Atomic Coordinates and Displacement Factors (pm^2) for $Mn_2(O_3PCH_2C_6H_4CH_2PO_3)\cdot 2H_2O$ (1)

Atom	Wyckoff pos.	x	y	z	U_{iso}[a]
Mn1	4a	0.1745(18)	0.503(4)	0.3798(9)	88(8)
Mn2	4a	− 0.0808(18)	0.001(5)	0.3998(9)	88(8)
P1	4a	− 0.2987(33)	0.990(6)	0.3084(13)	89(12)
P2	4a	0.4516(33)	0.500(7)	0.4704(14)	89(12)
O1	4a	− 0.4498(40)	0.986(14)	0.3196(17)	89(12)
O2	4a	− 0.2245(51)	0.802(6)	0.3442(24)	89(12)
O3	4a	− 0.2320(41)	0.184(5)	0.3448(21)	89(12)
O4	4a	0.2993(37)	0.497(14)	0.4621(17)	89(12)
O5	4a	0.5184(49)	0.685(6)	0.4309(22)	89(12)
O6	4a	0.5188(41)	0.311(5)	0.4321(19)	89(12)
O7	4a	0.0534(25)	0.474(9)	0.2891(11)	89(12)
O8	4a	− 0.2414(22)	0.015(17)	0.4775(12)	89(12)
C1	4a	− 0.256(7)	0.031(13)	0.2287(13)	89(12)
C2	4a	− 0.342(6)	0.911(11)	0.1799(31)	89(12)
C3	4a	− 0.269(6)	0.697(11)	0.1737(33)	89(12)
C4	4a	0.309(7)	0.442(10)	0.6234(29)	89(12)
C5	4a	0.428(6)	0.397(11)	0.5902(31)	89(12)
C6	4a	0.488(7)	0.178(11)	0.6028(29)	89(12)
C7	4a	− 0.452(6)	0.995(11)	0.1453(25)	89(12)
C8	4a	0.485(9)	0.583(11)	0.5488(13)	89(12)

[a] U_{iso} is defined as exp ($-8\pi^2 U_{iso} \sin^2 \theta/\lambda^2$).

X-Ray Structure Determination

The diffraction investigations were carried out on a conventional powder diffractometer (STOE Stadi P, Cu$K\alpha_1$ radiation for **2** and Mo$K\alpha$ radiation for **1** and **3**) in Debye–Scherrer geometry. The diffraction patterns were indexed by the program ITO (15), the space groups were determined by systematic extinction rules and they were confirmed by the successful structure refinement (Table 1). The diffraction patterns and the lattice constants of **1**–**3** are similar to those of $Co_2(O_3PCH_2C_6H_4CH_2PO_3)\cdot 2H_2O$ (14). Therefore, the atomic coordinates of $Co_2(O_3PCH_2C_6H_4CH_2PO_3)\cdot 2H_2O$, were used as starting parameters for the Rietveld refinements of **1**–**3** which were performed with the program GSAS (15). Starting from the atomic coordinates of $Co_2(O_3PCH_2C_6H_4CH_2PO_3)\cdot 2H_2O$, the Rietveld refinements were straightforward, but soft constraints for the distances *M*–O, P–O, P–C, and C–C were used. The atomic

TABLE 3
Atomic Coordinates and Displacement Factors (pm²) for $Ni_2(O_3PCH_2C_6H_4CH_2PO_3)\cdot 2H_2O$ (2)

Atom	Wyckoff pos.	x	y	z	U_{iso}[a]
Ni1	4a	0.1680(11)	0.4870(24)	0.3829(7)	276(15)
Ni2	4a	0.8997(10)	0.0052(29)	0.4003(7)	276(15)
P1	4a	0.6816(18)	0.995(5)	0.3200(10)	245(28)
P2	4a	0.4611(16)	0.484(4)	0.4645(10)	245(28)
O1	4a	0.5259(21)	0.953(7)	0.3229(12)	186(28)
O2	4a	0.7717(30)	0.792(4)	0.3428(15)	186(28)
O3	4a	0.7551(33)	0.210(4)	0.3464(16)	186(28)
O4	4a	0.3088(20)	0.531(8)	0.4538(13)	186(28)
O5	4a	0.5152(33)	0.710(4)	0.4350(16)	186(28)
O6	4a	0.5224(33)	0.281(4)	0.4271(16)	186(28)
O7	4a	0.0234(27)	0.532(8)	0.3030(13)	186(28)
O8	4a	0.7347(29)	−0.030(9)	0.4715(13)	186(28)
C1	4a	0.727(6)	0.065(9)	0.2415(10)	280(60)
C2	4a	0.659(6)	0.948(11)	0.1868(22)	280(60)
C3	4a	0.720(6)	0.728(10)	0.1682(25)	280(60)
C4	4a	0.323(7)	0.437(9)	0.6225(26)	280(60)
C5	4a	0.447(6)	0.360(9)	0.5918(23)	280(60)
C6	4a	0.510(5)	0.143(9)	0.6132(23)	280(60)
C7	4a	0.548(6)	1.039(8)	0.1504(26)	280(60)
C8	4a	0.520(5)	0.511(11)	0.5433(11)	280(60)

[a] U_{iso} is defined as $\exp(-8\pi^2 U_{iso}\sin^2\theta/\lambda^2)$.

coordinates of the compounds are listed in Tables 2–4, the refined powder diffraction patterns are shown in Figs. 1–3 (16).

TABLE 4
Atomic Coordinates and Displacement Factors (pm²) for $Cd_2(O_3PCH_2C_6H_4CH_2PO_3)\cdot 2H_2O$ (3)

Atom	Wyckoff pos.	x	y	z	U_{iso}[a]
Cd1	4a	0.1798(5)	0.4867(12)	0.3754(5)	183(2)
Cd2	4a	−0.0790(6)	−0.0085(15)	0.4000(5)	183(2)
P1	4a	−0.3065(15)	1.0087(34)	0.3073(8)	183(2)
P2	4a	0.4659(15)	0.4956(47)	0.4628(9)	183(2)
O1	4a	−0.4520(18)	0.9736(89)	0.3159(10)	183(2)
O2	4a	−0.2274(20)	0.8034(27)	0.3243(7)	183(2)
O3	4a	−0.2416(22)	0.1776(26)	0.3485(11)	183(2)
O4	4a	0.3219(18)	0.5479(53)	0.4540(11)	183(2)
O5	4a	0.5293(28)	0.7024(38)	0.4355(11)	183(2)
O6	4a	0.5382(22)	0.2834(31)	0.4450(8)	183(2)
O7	4a	0.0224(20)	0.5019(110)	0.2973(9)	183(2)
O8	4a	−0.2548(18)	−0.0162(80)	0.4693(9)	183(2)
C1	4a	−0.238(4)	0.033(9)	0.2316(9)	183(2)
C2	4a	−0.328(5)	0.928(7)	0.1846(18)	183(2)
C3	4a	−0.265(5)	0.722(7)	0.1714(22)	183(2)
C4	4a	0.316(6)	0.420(6)	0.6253(24)	183(2)
C5	4a	0.429(5)	0.340(8)	0.5942(21)	183(2)
C6	4a	0.497(5)	0.138(7)	0.6078(21)	183(2)
C7	4a	−0.437(5)	1.007(8)	0.1502(20)	183(2)
C8	4a	0.476(4)	0.498(9)	0.5450(9)	183(2)

[a] U_{iso} is defined as $\exp(-8\pi^2 U_{iso}\sin^2\theta/\lambda^2)$.

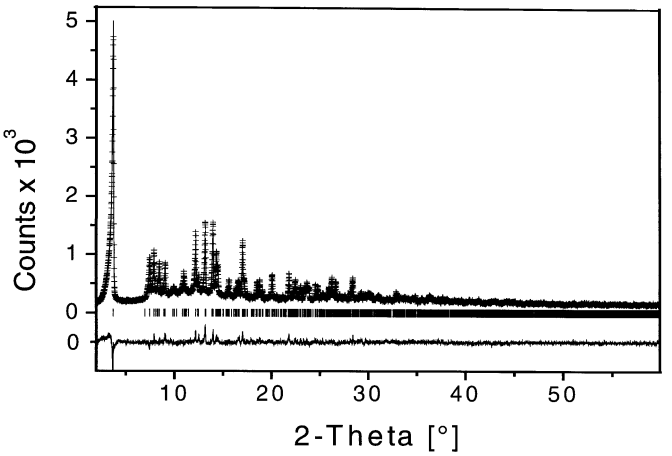

FIG. 1. Observed (+ + +) and calculated (—) X-ray powder diffraction pattern as well as difference profile of the Rietveld refinement of $Mn_2(O_3PCH_2C_6H_4CH_2PO_3)\cdot 2H_2O$ (**1**) (STOE Stadi P, $\lambda = 70.930$ pm). The row of vertical lines indicates possible peak positions.

RESULTS AND DISCUSSION

X-Ray Crystal Structure

All three title compounds $M_2(O_3PCH_2C_6H_4CH_2PO_3)\cdot 2H_2O$ (M = Mn, Ni, Cd) have been obtained as single-phase microcrystalline products. The asymmetric unit contains two metals, two phosphorus, eight oxygen and eight carbon atoms. The coordination geometry is very similar to that observed for $M(O_3PC_6H_5)$ (M = Mg, Mn, Zn, Ca, Cd) (17). The common features of the three isostructural compounds are corner-linked $[MO_6]$ polyhedra forming layers perpendicular to [001] (Fig. 4). Each metal ion is

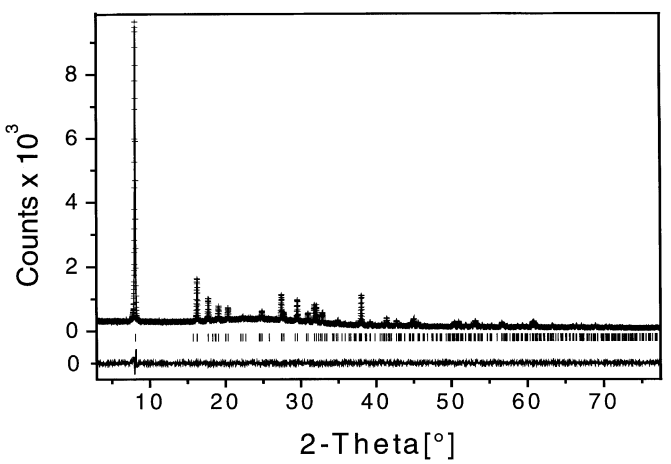

FIG. 2. Observed (+ + +) and calculated (—) X-ray powder diffraction pattern as well as difference profile of the Rietveld refinement of $Ni_2(O_3PCH_2C_6H_4CH_2PO_3)\cdot 2H_2O$ (**2**) (STOE Stadi P, $\lambda = 154.06$ pm). The row of vertical lines indicates possible peak positions.

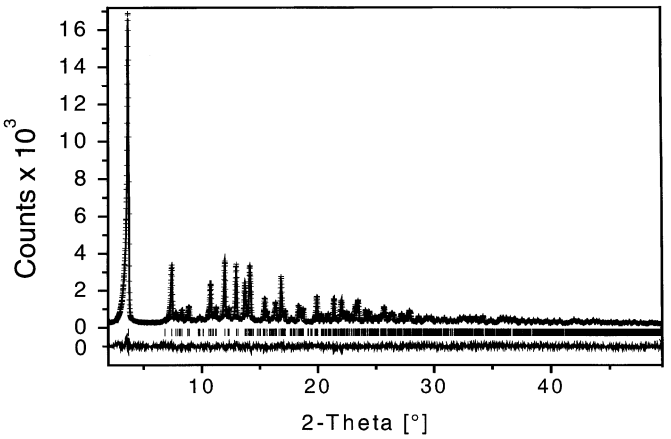

FIG. 3. Observed (+ + +) and calculated (—) X-ray powder diffraction pattern as well as difference profile of the Rietveld refinement of $Cd_2(O_3PCH_2C_6H_4CH_2PO_3)\cdot 2H_2O$ (**3**) (STOE Stadi P, $\lambda = 70.930$ pm). The row of vertical lines indicates possible peak positions.

surrounded by five phosphonate oxygen atoms and one water molecule (O7 and O8 for $M1$ and $M2$, respectively (M = Mn, Ni, Cd)) and the phosphonate groups coordinate four metal ions. As observed in $M(O_3PC_6H_5)$ (M = Mg, Mn, Zn, Ca, Cd) (17), two oxygen atoms of the phosphonate groups chelate to the metal while at the same time, the chelating oxygens bridge the adjacent metal atoms (Fig. 4). The M–O layers are located at $z \sim 0.4$ and 0.9 and are pillared by the *p*-xylenediphosphonate groups (Fig. 5). An ABAB-type stacking of the phenyl rings along [001] is observed. Due to the presence of the $-CH_2-$ groups, the

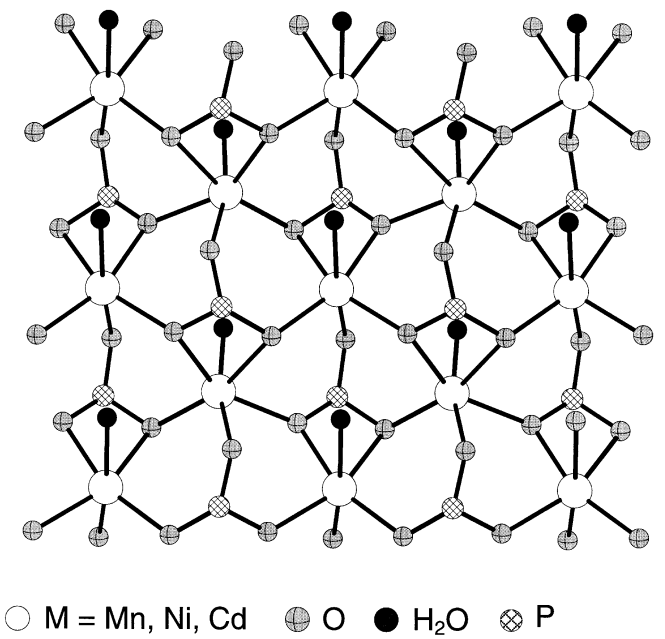

FIG. 4. Corner-linked [MO_6] polyhedra in $M_2(O_3PCH_2C_6H_4CH_2PO_3)\cdot 2H_2O$ (M = Mn, Ni, Cd). View along [001].

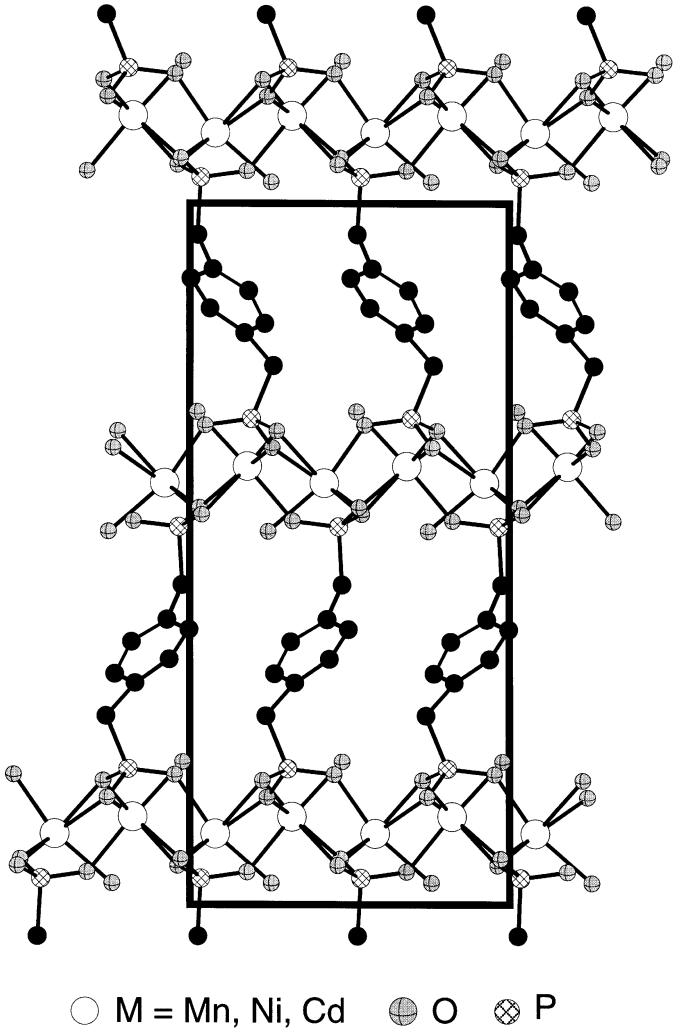

FIG. 5. Pillared structure of $M_2(O_3PCH_2C_6H_4CH_2PO_3)\cdot 2H_2O$ (M = Mn, Ni, Cd). View along [100].

phenyl rings are tilted by 45(1), 41(1) and 49(1)° for **1**–**3**, respectively, with respect to the perpendicular axis at the layer plane. The phenyl rings in the xy plane are parallel along the [010]-axis. Due to a glide plane, the phenyl rings along [100] are tilted in respect to each other by approximately 50°. This is in contrast to the findings in $Cu_2(O_3PCH_2C_6H_4CH_2PO_3)\cdot 2H_2O$, where the phenyl rings in one layer are only slightly tilted with respect to each other and form an AAAA-type stacking.

According to the ionic radii for hexacoordinated metal ions (Ni^{2+}: 69.0, Mn^{2+}: 83.0, Cd^{2+}: 95.0 pm) (18), a gradual increase of the a and b lattice constants in the order Ni < Mn < Cd from $a = 951.18(3)$ to 1005.19(3) pm and $b = 562.31(2)$ to 594.37(2) pm for $Ni_2(O_3PCH_2C_6H_4CH_2PO_3)\cdot 2H_2O$ and $Cd_2(O_3PCH_2C_6H_4CH_2PO_3)\cdot 2H_2O$, respectively, is observed. In contrast, only minor changes of the c lattice constant are found varying from 2173.5(2) to 2186.08(8) pm for **1** and **3**, respectively.

TABLE 5
Interatomic Distances (pm) in $Mn_2(O_3PCH_2C_6H_4CH_2PO_3)\cdot 2H_2O$ (1)

	MnO_6 polyhedra		
Mn1–O2	218.1(6)	Mn2–O1	217.0(5)
Mn1–O3	218.1(6)	Mn2–O2	219.2(6)
Mn1–O4	216.9(6)	Mn2–O3	218.5(6)
Mn1–O5	218.7(6)	Mn2–O5	218.2(5)
Mn1–O6	219.2(6)	Mn2–O6	218.4(6)
Mn1–O7	231.0(4)	Mn2–O8	231.3(4)
	PO_3C polyhedra		
P1–O1	150.6(4)	P2-O4	150.9(5)
P1–O2	152.5(6)	P2–O5	152.4(5)
P1–O3	152.8(6)	P2–O6	153.0(6)
P1–C1	180.1(4)	P2–C8	180.2(4)
	Xylene group		
C1–C2	152.7(8)	C5-C8	151.6(7)
C2–C3	144.7(13)	C5–C6	143.0(10)
C3–C4	141.6(9)	C6–C7	141.4(7)
C4–C5	140.4(5)	C7–C2	140.9(5)

TABLE 7
Interatomic Distances (pm) in $Cd_2(O_3PCH_2C_6H_4CH_2PO_3)\cdot 2H_2O$ (3)

	CdO_6 polyhedra		
Cd1–O2	225.6(8)	Cd2–O1	224.8(8)
Cd1–O3	222.5(8)	Cd2–O2	249.3(4)
Cd1–O4	226.3(8)	Cd2–O3	227.3(8)
Cd1–O5	229.7(8)	Cd2–O5	225.7(8)
Cd1–O6	249.1(4)	Cd2–O6	224.1(8)
Cd1–O7	233.0(8)	Cd2–O8	232.8(8)
	PO_3C polyhedra		
P1–O1	148.9(4)	P2–O4	149.3(4)
P1–O2	150.3(4)	P2–O5	150.8(4)
P1–O3	149.8(4)	P2–O6	150.7(4)
P1–C1	179.7(4)	P2–C8	179.9(4)
	Xylene group		
C1–C2	150.3(4)	C5–C8	150.6(4)
C2–C3	141.0(4)	C5–C6	140.7(4)
C3–C4	140.2(4)	C6–C7	140.6(4)
C4–C5	140.8(4)	C7–C2	140.9(4)

The trends observed for the lattice constants are due to the metal-oxygen distances. The smallest metal-oxygen distances are observed in $Ni_2(O_3PCH_2C_6H_4CH_2PO_3)\cdot 2H_2O$ (**2**). The Ni–O distances to the phosphonate groups and the water molecules 205(2)–215(2) pm/223(2), 222(2) pm, respectively, are in agreement with the values observed for other nickeldiphosphonates (195(3)–226(3) pm) and within the range of the sum of the ionic radii Ni^{2+} and O^{2-} (83 + 122 = 205 pm) (18). The distances Mn–O to the phosphonate groups and the water molecules of 216.9(6)–219.2(6) pm/231.0(4), 231.3(4) pm, respectively, are approximately 10 pm longer and agree well with values observed in other manganese phosphates ($Mn_2(PO_4)(OH)$: d (Mn–O) = 210.9–223.5 pm, β'-$Mn_3(PO_4)_2$: d (Mn–O) = 212.6–224.2 pm) and with the sum of the ionic radii Mn^{2+} and O^{2-} (97 + 122 = 219 pm) (18). As expected, the largest metal–oxygen bonds are found in $Cd_2(O_3PCH_2C_6H_4CH_2PO_3)\cdot 2H_2O$, where the distances Cd–O to the phosphonate groups and the water molecules are 222.5(8)–249.3(4) pm/233.0(8), 232.8(8) pm, respectively. Thus, a larger variation of M–O distances is observed, but these results are in agreement with the values observed in $Cd(O_3PCH_2CH_2NH_2)$ (195(3)–226(3) pm) (19) and with the sum of the ionic radii Cd^{2+} and O^{2-} (109 + 122 = 231 pm) (18). In contrast to the expected large variations of the M–O distances, only minor differences are observed in the P–O, P–C, CH_2–C, and C=C distances (20) (see Tables 5–7).

TABLE 6
Interatomic Distances (pm) in $Ni_2(O_3PCH_2C_6H_4CH_2PO_3)\cdot 2H_2O$ (2)

	NiO_6 polyhedra		
Ni1–O2	205(2)	Ni2–O1	208(2)
Ni1–O3	206(2)	Ni2–O2	212(2)
Ni1–O4	206(2)	Ni2–O3	214(2)
Ni1–O5	215(2)	Ni2–O5	209(2)
Ni1–O6	213(2)	Ni2–O6	207(2)
Ni1–O7	223(2)	Ni2–O8	222(2)
	PO_3C polyhedra		
P1–O1	150(2)	P2–O4	149(2)
P1–O2	151(2)	P2–O5	151(2)
P1–O3	151(2)	P2–O6	152(2)
P1–C1	181(2)	P2–C8	181(2)
	Xylene group		
C1–C2	151(2)	C5–C8	152(2)
C2–C3	143(2)	C5–C6	144(2)
C3–C4	142(2)	C6–C7	141(2)
C4–C5	143(2)	C7–C2	142(2)

IR Spectroscopy

The IR spectra of the three title compounds are almost identical, thus only the spectrum of $Mn_2(O_3PCH_2C_6H_4CH_2PO_3)\cdot 2H_2O$ (**1**) will be discussed (Fig. 6). Two bands at 3491 and 3421 cm^{-1} are due to the asymmetric and symmetric O–H stretching vibrations of the hydration water. The corresponding deformation vibration $\delta(H_2O)$ is observed at 1601 cm^{-1}. The sharp band at 3052 cm^{-1} is characteristic of the C–H stretching vibration of the phenyl ring and the bands between 2917 and 3024 cm^{-1} can be attributed to the asymmetric and symmetric C–H stretching vibrations of the $-CH_2$ groups. The IR spectrum is typical for a *para*-substituted benzene ring (21). Three

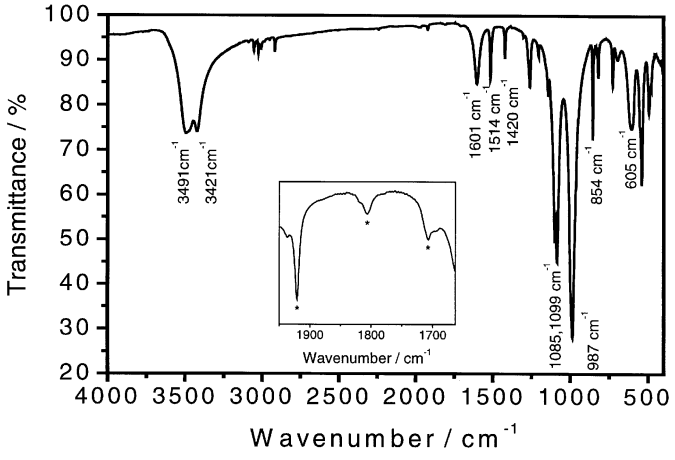

FIG. 6. IR spectrum of $Mn_2(O_3PCH_2C_6H_4CH_2PO_3)\cdot 2H_2O$ (**1**).

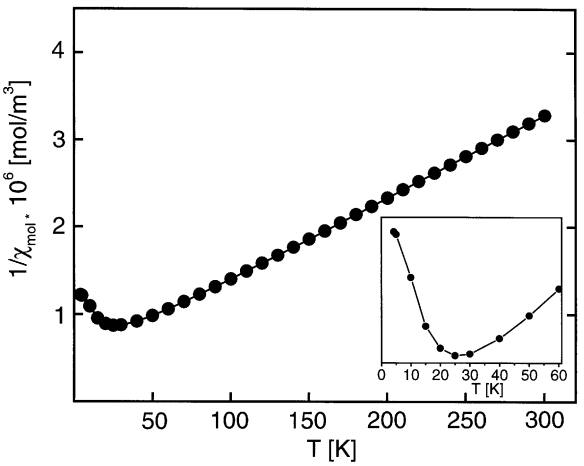

FIG. 7. The inverse molar magnetic susceptibility of polycrystalline $Mn_2(O_3PCH_2C_6H_4CH_2PO_3)\cdot 2H_2O$ (**1**) plotted as a function of the temperature (4–300 K).

skeletal ring vibration modes are expected, but only two at 1420 and 1514 cm^{-1} can be observed. The third band expected around $\sim 1600\,cm^{-1}$ is either covered by the broad band of the $\delta(H_2O)$ vibration or it has only a very low intensity. The latter is supported by IR investigations of the free *p*-xylenediphosphonic acid (14). As expected for *para*-substituted benzene rings, one sharp δ(CH) out-of-plane vibration at 854 cm^{-1} is found. The region between 2000 and 1650 cm^{-1} shows the pattern of three bands (overtone and combination bands at 1920, 1807, 1708 cm^{-1}) characteristic for *para*-substituted benzene rings (inset of Fig. 6). The set of bands between 1200 and 900 cm^{-1} is due to stretching vibrations of the tetrahedral CPO_3 groups and the band centered at $605\,cm^{-1}$ can be assigned to δ(Mn–O–H), by analogy with the observations in $MnAsO_4\cdot 1.2H_2O$ (22) and $MnPO_4\cdot H_2O$ (23). While the bands associated with the organic part of the structure are located at very similar wavenumbers ($\pm 5\,cm^{-1}$), bands which are due to vibrations involving the $[CPO_3]$ and $[MO_6]$ polyhedra show larger variations (up to $\pm 70\,cm^{-1}$).

Magnetic Properties

Figure 7 shows the inverse magnetic susceptibility of $Mn_2(O_3PCH_2C_6H_4CH_2PO_3)\cdot 2H_2O$ (**1**) plotted as a function of temperature. At higher temperatures, the compound exhibits Curie–Weiss behavior. The data were least-squares fitted to a Curie–Weiss equation $\chi_M = C/(T-\theta)$ yielding $\theta = -44.1$ K and the effective magnetic moment μ_{eff} per metal atom of 5.77 μ_B was obtained. This value is only slightly smaller than the ideal value of 5.92 μ_B for a high-spin d^5 system and compares well to values observed in other studies. At lower temperatures, **1** undergoes an antiferromagnetic ordering transition at 25 K (see inset) which is consistent with its negative Weiss constant. The antiferromagnetic behavior was also confirmed by measuring the magnetization vs. applied field curve at 20 K.

ACKNOWLEDGMENTS

Norbert Stock thanks Galen Stucky for the opportunity to work in his group as a Post-Doc in 1999. Thomas Bein thanks Galen Stucky for a fruitful and interesting time in his research group at DuPont Central Research (1984–85) and for many years of enjoyable collaborations and discussions. The authors thank E. Irran for the helpful discussion regarding the Rietveld refinements, R. Pöttgen and Dr. G. Kotzyba for the magnetic and E. Kiesewetter for the IR measurements.

REFERENCES

1. A. K. Cheetham, G. Férey, and T. Loiseau, *Angew. Chem.* **111,** 3466 (1999); *Angew. Chem. Int. Ed.* **38,** 3268 (1999).
2. (a) A. Clearfield, *Chem. Mater.* **10,** 2801 (1998); (b) M. B. Dines and P. M. DiGiacomo, *Inorg. Chem.* **20,** 92 (1981).
3. (a) A. Distler, D. L. Lohse, and S. C. Sevov, *J. Chem. Soc. Dalton Trans.* 1805 (1999); (b) V. Soghomonian, Q. Chen, R. C. Haushalter, and J. Zubieta, *Angew. Chem. Int. Ed.* **34,** 223 (1995); c) C. Serre and G. Férey, *Inorg. Chem.* **38,** 5370 (1999); d) R. LaDuca, D. Rose, J. R. D. DeBord, R. C. Haushalter, C. J. O'Connor, and J. Zubieta, *J. Solid State Chem.* **123,** 408 (1996); D. L. Lohse and S. C. Sevov, *Angew. Chem., Int. Ed.* **36,** 1619 (1997).
4. S. Drumel, P. Janvier, D. Deniaud, and B. Bujoli, *J. Chem. Soc., Chem. Commun.* 1051 (1995).
5. (a) N. Stock, S. A. Frey, G. D. Stucky, and A. K. Cheetham, *J. Chem. Soc. Dalton Trans.* 4292 (2000); (b) N. Stock, and G. D. Stucky, A. K. Cheetham, *J. Chem. Soc. Chem. Commun.* 2277 (2000); (c) S. Drumel, M. Bujoli-Doeuff, P. Janvier, and B. Bujoli, *New J. Chem.* **19**(3), 239 (1995).
6. A. Clearfield, *Curr. Opin. Solid State Mater. Sci.* **1,** 268 (1996); G. Alberti, *Compr. Supramol. Chem.* **7,** 151 (1996).
7. (a) D. Riou, F. Belier, C. Serre, M. Noguès, D. Vichard, and G. Férey, *Int. J. Inorg. Mater.* **2,** 29 (2000); (b) D. M. Poojary, B. Zhang, and A. Clearfield, *J. Am. Chem. Soc.* **119,** 12550 (1997); (c) D. M. Poojary, B. Zhang, P. Bellinghausen, and A. Clearfield, *Inorg. Chem.* **35,** 5254 (1996).
8. M. Riou-Cavellec, C. Serre, J. Robino, M. Noguès, J.-M. Grenèche, and G. Férey, *J. Solid State Chem.* **147,** 122 (1999).

9. D. M. Poojary, B. Zhang, and A. Clearfield, *An. Quim. Int. Ed.* **94**(6), 401 (1998).
10. K. Barthelet, C. Jouve, D. Riou, and G. Férey, *Solid State Sci.* **2,** 871 (2000).
11. C. V. K. Sharma, A. Clearfield, A. Cabeza, M. A. G. Aranda, and S. Bruque, *J. Am. Chem. Soc.* **123,** 2885 (2001).
12. Q. Gao, N. Guillou, M. Noguès, A. K. Cheetham, and G. Férey, *Chem. Mater.* **11,** 2937 (1999).
13. N. A. Caplan, C. I. Pogson, D. J. Hayes, and G. M. Blackburn, *J. Chem. Soc., Perkin Trans.* **1,** 421 (2000).
14. N. Stock and T. Bein, in preparation.
15. A. C. Larson and R. B. von Dreele, General Structure Analysis System, Los Alamos National Laboratory Report, LAUR 86-748. 1990.
16. Crystallographic data (excluding structure factors) for the structures in this paper have been deposited with the Cambridge Crystallographic Data Centre as supplementary publication nos. CCDC-180600 ($Mn_2[O_3P–CH_2–C_6H_4–CH_2–PO_3]\cdot 2H_2O$), CCDC-180601 ($Ni_2[O_3P–CH_2–C_6H_4–CH_2–PO_3]\cdot 2H_2O$) and CCDC-180602 ($Cd_2[O_3P–CH_2–C_6H_4–CH_2–PO_3]\cdot 2H_2O$). Copies of the data can be obtained, free of charge, on application to CCDC, 12 Union Road, Cambridge CB2 1EZ, UK (fax: +44 1223 336033 or e-mail: deposit@ccdc.cam.ac.uk).
17. G. Cao, H. Lee, V. M. Lynch, and T. E. Mallouk, *Inorg. Chem.* **27,** 2781 (1988).
18. R. D. Shannon, *Acta Crystallogr. A* **32,** 751 (1976).
19. F. Fredoueil, D. Massiot, P. Janvier, F. Gingl, M. Bujoli-Doeuff, M. Evain, A. Clearfield, and B. Bujoli, *Inorg. Chem.* **38,** 1831 (1999).
20. (**1**: P–O: 150.6(4)–153.0(6) pm, P–C: 180.1(4), 180.2(4) pm, CH_2–C:152.7(8), 151.6(7) pm, C=C: 140.4(5)–145(2) pm; **2**: P–O: 149(1)–152(2) pm, P–C: 181(2) pm, CH_2–C: 151(2), 152(2), C=C: 142(2)–144(2) pm; **3**: P–O: 148.9(4)–150.8(4) pm, P–C: 179.7(4), 179.9(4) pm, CH_2–C: 150.3(4), 150.6(4), C=C: 140.2(4)–141.0(4) pm. These values compare well with the ones for the free diphosphonic acid $H_2O_3P–CH_2–C_6H_4–CH_2–PO_3H_2$ (P–O: 149.3(2)–155.2(2) pm, P–C: 178.3(2) pm, CH_2–C: 150.7(2), 150.6(4), C=C: 138.1(2)–138.7(2) pm) (14). The larger bond distances P–O in the acid are due to the P–OH groups in the *p*-xylenediphosphonic acid.
21. L. J. Bellamy, "The Infrared Spectra of Complex Molecules," Chapmann & Hall, London, 1975.
22. M. A. G. Aranda, S. Bruque, and J. P. Attfield, *Inorg. Chem.* **30,** 2043 (1991).
23. M. A. G. Aranda and S. Bruque, *Inorg. Chem.* **29,** 1334 (1990).